Cement and Concrete Research 90 (2016) 117–126

Contents lists available at ScienceDirect

Cement and Concrete Research

journal homepage: www.elsevier.com/locate/cemconres

A micromechanics-based fatigue dependent fiber-bridging constitutive model

Jishen Qiu, En-Hua Yang *

Civil and Environmental Engineering, Nanyang Technological University, Singapore 639797, Singapore

ARTICLE INFO

Article history:
Received 12 April 2016
Received in revised form 2 September 2016
Accepted 21 September 2016
Available online 3 October 2016

Keywords:
Analytical model
Fatigue
FRCC
Micromechanics
PVA fiber
Single-fiber

ABSTRACT

Fiber-reinforced cementitious composites (FRCC) represent a large group of construction and building materials. While numerous experimental studies have been conducted on fatigue of FRCC, predicting FRCC fatigue performance remains difficult. This paper proposes a novel multi-scale analytical model to capture the fatigue dependency of fiber bridging constitutive law in FRCC. On the micro-scale, a new analytical model to predict the post-fatigue single-fiber pullout behavior (*P-u* curve) is established based on the understanding of the fatigue dependency of fiber and fiber-matrix interface. On the macro-scale, the fatigue-induced fiber strength reduction was considered and probabilistics is introduced to describe the randomness of fiber location and orientation so that the fatigue dependent fiber-bridging constitutive law can be predicted. The model proposed in this paper is the first analytical model that is able to capture the effects of fatigue cycle as well as the fatigue loading level on deterioration of fiber bridging in FRCC.

1. Introduction

Fatigue is an important factor for the deterioration of many reinforced concrete infrastructure, such as pavement [1], bridge [2], railway slippers [3], and the supporting structure of offshore windmills [4]. Under repeated loading, the intrinsic flaws and micro cracks in concrete would gradually propagate into macro cracks. This reduces not only the structural capacity and serviceability but also the durability as the aggressive acid rain or sea water would penetrate through the cracks. The coupling effect of load repetition and environmental attack greatly shorten the service life of these infrastructures.

Fibers provide effective means to suppress the brittleness of cement-based materials. Under repeated loading, fiber bridging of fiber-reinforced cementitious composites (FRCC) can effectively relieve the stress concentration at the crack tip, thus decelerating the crack propagation and extending the fatigue life of the structure [5]. The extension of fatigue life with increasing fiber content has been observed in FRCC reinforced by various types of fibers, such as steel fibers [6–8], polymeric fibers [9–11], glass fibers [12], and carbon fibers [13]. The effects of fiber dimension on fatigue life, however, remain controversial. For example, Johnston and Zemp [6], on the basis of fatigue test over 100 specimens, concluded that higher fiber aspect ratio, i.e. length-to-diameter ratio, led to higher flexural fatigue strength and extended fatigue life; while Naaman and Hammound [14] noticed in their tests that fiber aspect ratio of 60 and 100 produced similar flexural fatigue strength and fatigue life. Such disagreement indicates the complicacy involved in predicting the fatigue performance of FRCC.

The key to predict fatigue performance of FRCC lies in robust characterization of fatigue-induced crack propagation, the rate of which is determined by the crack-tip stress intensity factor. The crack-tip stress intensity factor is influenced by the quality of fiber bridging, which deteriorate continuously with fatigue loading [15]. Two models have been proposed to predict the fatigue-induced fiber-bridging deterioration of FRCC. In a force equilibrium-based model, Zhang et al. [16] measured the fiber-bridging law, i.e. the tensile stress vs. crack opening displacement curve, with notched cube specimens under tensile fatigue loading, so the fiber-bridging deterioration can be modelled analytically. The limitation of such method lies that micro-scale factors such as fiber geometry cannot be included and that fatigue tests must be conducted once the mix design is changed. In a fracture mechanics-based model, Li and Matsumoto [17,18] established the fiber-bridging law by summing the pullout behavior of individual fibers after fatigue deterioration. In their model, the frictional bond between fiber and matrix interface was assumed to decrease with fatigue cycles without any experimental justification. In addition, chemical adhesion between fibers and matrix was not considered.

Recently, the fatigue-induced fiber and fiber-matrix interfacial deterioration has been experimentally characterized and new deterioration mechanisms have been discovered in a micro-polyvinyl alcohol (PVA) fiber reinforced cementitious composites by the authors [19,20]. To characterize fiber deterioration under fatigue, single PVA fiber was embedded in cement matrix with large embedment length to prevent full debonding of fiber from the matrix. The embedded fiber with different inclination angle underwent tensile fatigue loading at various loading

* Corresponding author at: N1-01b-56, 50 Nanyang Avenue, 639798, Singapore.
E-mail address: ehyang@ntu.edu.sg (E.-H. Yang).

http://dx.doi.org/10.1016/j.cemconres.2016.09.017
0008-8846/

level until fiber rupture. It was found that the in-situ strength of PVA fiber decreased with increasing load cycles. To investigate deterioration of fiber-matrix interface properties, single PVA fiber was embedded in cement matrix with small embedment length so that fiber underwent debonding and sliding from the surrounding cement matrix when subjected to tensile fatigue loading. It was discovered that fatigue load was able to propagate the tunnel crack along the fiber-matrix interface, which was referred as fatigue-induced fiber debonding, and an empirical relation between debonding rate and fatigue loading level similar to the Paris' law was suggested. It was observed that interface chemical bond Gd was fatigue independent while frictional bond τ0 increased with fatigue cycles N and fatigue loading levels Pmax. Such fatigue-induced interface hardening can occur during fiber debonding stage, which was referred as fatigue debonding hardening, as well as during fiber slippage stage, which was referred as fatigue slippage hardening. These phenomena led to premature fiber rupture and may cause severe fiber-bridging deterioration, which needs to be captured with proper model.

In this paper, a micromechanics-based fatigue dependent fiber-bridging constitutive model was proposed by taking account of fatigue dependency in material microstructure which consists of fiber, matrix, and fiber-matrix interface. Parametric study on the influence of fatigue loading level and fatigue cycle as well as fiber surface treatment on the fiber-bridging σ-δ curves was also reported and discussed.

2. Modeling approach: Scale linking

Scale linking represents the approach behind the development of current model as shown in Fig. 1. As can be seen, fibers bridge across the crack and fiber-bridging spring law governs the bridging behavior in the macro-scale (μm–mm). One scale below is the material microstructure (nm–μm) which consists of fiber, matrix, and fiber-matrix interface. This conceptual illustration suggests that performance of fiber bridging in the macro-scale is governed by the properties of component, i.e. fiber, matrix, and interface, in the micro-scale. Specifically, deterioration of the fiber-bridging constitutive law subject to fatigue is a result of fatigue dependencies in fiber, matrix, and fiber-matrix interface micro-scale.

The fatigue dependent stress-crack opening relationship $\sigma(\delta)$, which can be viewed as the constitutive law of fiber-bridging behavior subject to fatigue, is derived by using analytic tools of fracture mechanics, micromechanics, and probabilistics. In particular, the energetics of tunnel crack propagation along fiber-matrix due to fatigue is used to quantify the fatigue-induced debonding process and fatigue-induced changes on the fiber and the fiber-matrix interfacial properties are captured in the micro-scale. The total stress carried across a crack is a composite action of many fibers bridging across this crack which can be express as a summation of the forces induced by each bridging fiber across the matrix crack per unit area. Probabilistics is introduced to describe the randomness of fiber location and orientation with respect to a crack plane. The random orientation of fiber also necessitates the accounting of the mechanics of interaction between an inclined fiber and the matrix crack. As a result, the $\sigma(\delta)$ curve is expressible as a function of fatigue dependent micromechanical parameters.

3. Micro-scale modeling: Fatigue dependent single-fiber pullout behavior

When a fiber is monotonically pulled out from the matrix, tunnel crack propagation along the fiber-matrix interface starts until the fiber is fully debonded from matrix followed by slippage of fiber out of the tunnel [21]. As shown in Fig. 2, the event of complete debonding (noticed by the sudden load drop from P_a to P_b) divides the single fiber pullout curve into the preceding fiber debonding stage and the following fiber slippage stage.

Based on fracture mechanics-based approach, Lin et al. [22,23] developed an analytical model for monotonic single fiber pullout force-displacement (P-u) relation, as explicitly expressed in Eqs. 1 to 4. In the fiber debonding stage (Eq. 1), the load P is resisted by the chemical bond G_d at the bonded interface as well as the frictional bond τ_0 at the debonded interface. After full debonding, i.e. in the fiber slippage stage, chemical bond diminishes and only the frictional bond dominates pullout behavior (Eq. 2). In this stage, due to the large relative displacement between soft fiber and hard matrix, the fiber surface is abraded and roughened, resulting in stronger friction. Such slippage-induced friction

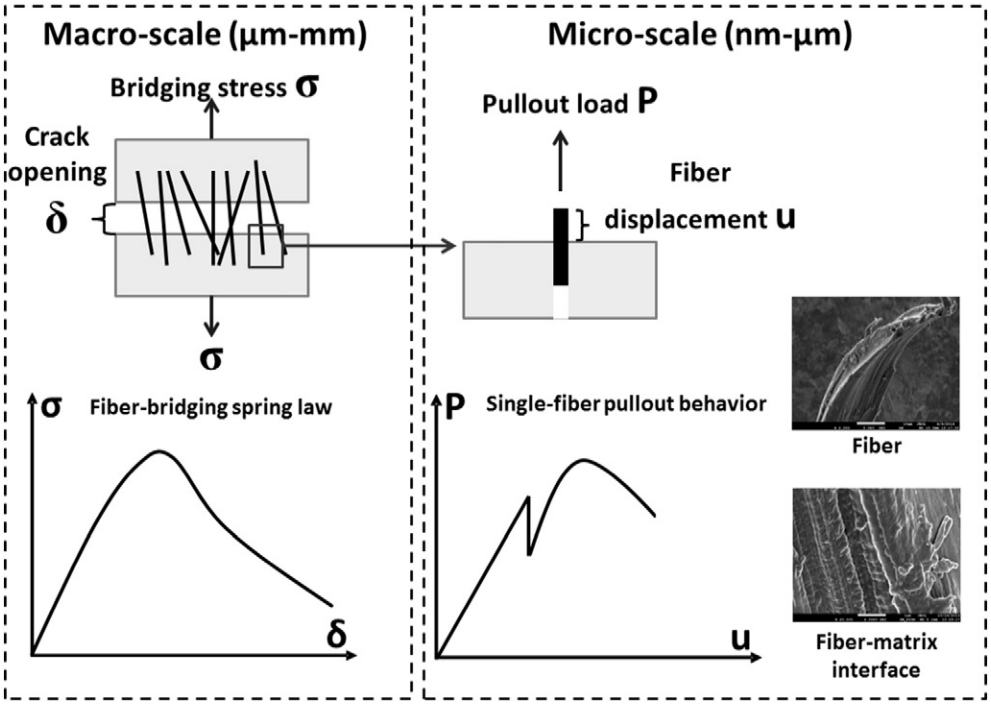

Fig. 1. Illustration of the scale linking in current model.

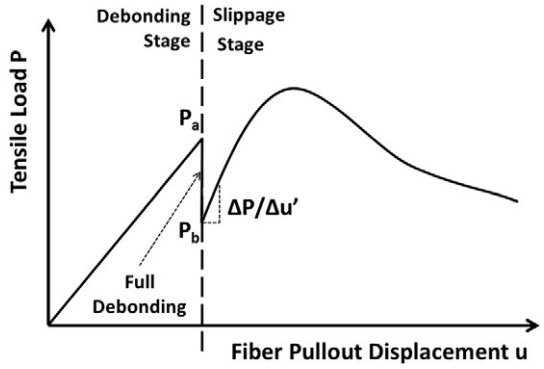

Fig. 2. Illustration of typical tensile load-displacement (P-u) curve in single-fiber pullout test.

increase is referred as slip hardening, and slip hardening coefficient β is introduced into the model (Eq. 3).

$$P = \sqrt{\frac{\pi^2(\tau_0 u + G_d)E_f d_f^3(1+\eta)}{2}}, \quad u \le u_0 \tag{1}$$

$$P = \frac{\pi\tau}{d_f}(L_e + u_0 - u), \quad u \ge u_0 \tag{2}$$

$$\tau = \tau_0\left[1 + \frac{\beta(u-u_0)}{d_f}\right] \tag{3}$$

$$u_0 = \frac{2\tau_0 L_e^2(1+\eta)}{E_f d_f} + \frac{L_e}{E_f}\sqrt{\frac{8G_d E_f(1+\eta)}{d_f}} \tag{4}$$

where E_f is the fiber Young's modulus; d_f is the fiber diameter; L_e is the fiber embedment length; u_0 is the displacement at full debonding; and $\eta = E_f V_f / E_m(1 - V_f)$ where E_m is the matrix Young's modulus and V_f is the fiber content by volume. At low fiber content, η approaches to zero.

The chemical bond G_d, frictional bond τ_0, and slip hardening coefficient β can be determined from the single-fiber pullout tests as shown in Eqs. 5 to 7.

$$G_d = \frac{2(P_a - P_b)^2}{\pi^2 E_f d_f^3} \tag{5}$$

$$\tau_0 = \frac{P_b}{\pi d_f L_e} \tag{6}$$

$$\beta = \frac{d_f}{L_e}\left(1 + \frac{1}{\pi\tau_0 d_f}\cdot\frac{\Delta P}{\Delta u'}\bigg|_{u'\to 0}\right) \tag{7}$$

where u' is the fiber displacement after full-debonding, and $\Delta P/\Delta u'$ is the initial slope of the P versus u' curve (u' approaching 0 as shown in Fig. 2).

To capture the fatigue dependency, the effects of fatigue loading, including *fatigue-induced fiber debonding*, *fatigue debonding hardening*, and *fatigue slippage hardening*, on single fiber pullout behavior are quantitatively characterized and incorporated into the new model. Specifically, fatigue loading level P_{max} and fatigue cycle N are included in this model and the influence of P_{max} and N on post-fatigue single fiber pullout curve, i.e. $P(u, P_{max}, N)$ is presented here.

3.1. Fatigue dependent fiber debonding process

In the fatigue single fiber pullout experiment of [20] where a micro-PVA fiber was pulled out from a mortar matrix, it has been shown that when the fatigue loading level P_{max} was much lower than the P_a, the full-debonding of fiber could not be reached during fatigue loading. The fatigue deterioration in the debonding stages can be characterized with such cases. Specifically, the *fatigue-induced fiber debonding* and *fatigue debonding hardening* must be added into the new model.

3.1.1. Fatigue-induced fiber debonding

The phenomenon of *fatigue-induced fiber debonding* has been observed in the debonding stage of single fiber pullout tests when the fatigue loading level P_{max} was smaller than P_a [20]. In the monotonic model, the interfacial debonding crack propagates only when the surface energy G, the energy released by creation of new crack surface per unit area, is equal to the chemical bond between fiber and matrix G_d. When the interface debonds, the relation between tensile load P and debonding crack length a is given based on Type II fracture criterion as

$$P = \pi\tau_0 a(1+\eta)d_f + \sqrt{\pi^2 G_d E_f(1+\eta)d_f^3/2} \tag{8}$$

where d_f is the fiber diameter, E_f is the Young's modulus of the fiber, $\eta = E_f V_f / E_m(1 - V_f)$, where E_m is the Young's of the matrix, and V_f is the fiber fraction by volume. Based on the equilibrium of the fiber-matrix system, the correlation between P, a, and fiber displacement u is obtained as Eq. 9:

$$P = \pi E_f d_f^2 u/4a + \pi\tau_0 a(1+\eta)d_f/2 \tag{9}$$

P-u relation in the debonding stage can be obtained once the crack length a is determined. The derivation of Eqs. 8 and 9 can be found in [22].

In current model, the debonding crack length a is composed of a_0, the crack length at the peak of the first load cycle and Δa, the crack propagation induced by fatigue loads (Eq. 10).

$$a = \min.\begin{cases} a_0 + \Delta a\,(N_d, P_{max}) \\ L_e \end{cases} \tag{10}$$

where N_d is the number of fatigue load cycles applied before during the debonding stage. In Eq. 10, a_0 can be calculated with Eq. 8 by substituting P with P_{max} and $\Delta a\,(N_d, P_{max})$ can be experimentally determined as illustrated Fig. 3 where a micro-PVA fiber was pulled out from a mortar matrix [20]. As can be seen in Fig. 3a, Δa increases with N as well as P_{max}. The *fatigue-induced fiber debonding* rate, i.e. the slope of the Δa-N curve, as shown in Fig. 3b increases with the increase of P_{max}, which can be described by a power function similar to the form of the Paris' Law [24] as Eq. 11 [16].

$$\Delta a = \max.\begin{cases} 0 \\ N_d \cdot C \cdot (P_{max} - P_0)^M \end{cases} \tag{11}$$

where C and M are material related constants, and P_0 is the threshold to initiates fatigue-induced fiber debonding. P_0 is determined by assuming a equals to zero in Eq. 8 and it can be calculated with Eq. 1 taking u=0. This specific data point is also considered in Fig. 3b in additional to the experimental results. The details of the single fiber fatigue pullout experimental program and discussions on the *fatigue-induced fiber debonding* rate can be found in [20].

3.1.2. Fatigue debonding hardening

At low-level fatigue ($P_{max} << P_a$), it was found that while the chemical bond G_d between fiber and matrix was not affected by fatigue loading, the frictional bond τ_0 was enhanced with fatigue cycle N_d and fatigue loading level P_{max} [20]. Such enhancement was referred as *fatigue debonding hardening*. This phenomenon is believed to be related to the damage of soft polymeric fiber caused by the reciprocated movement of debonded fiber portion against hard cement matrix subject to fatigue. A jamming effect can take place inside the matrix due to fiber

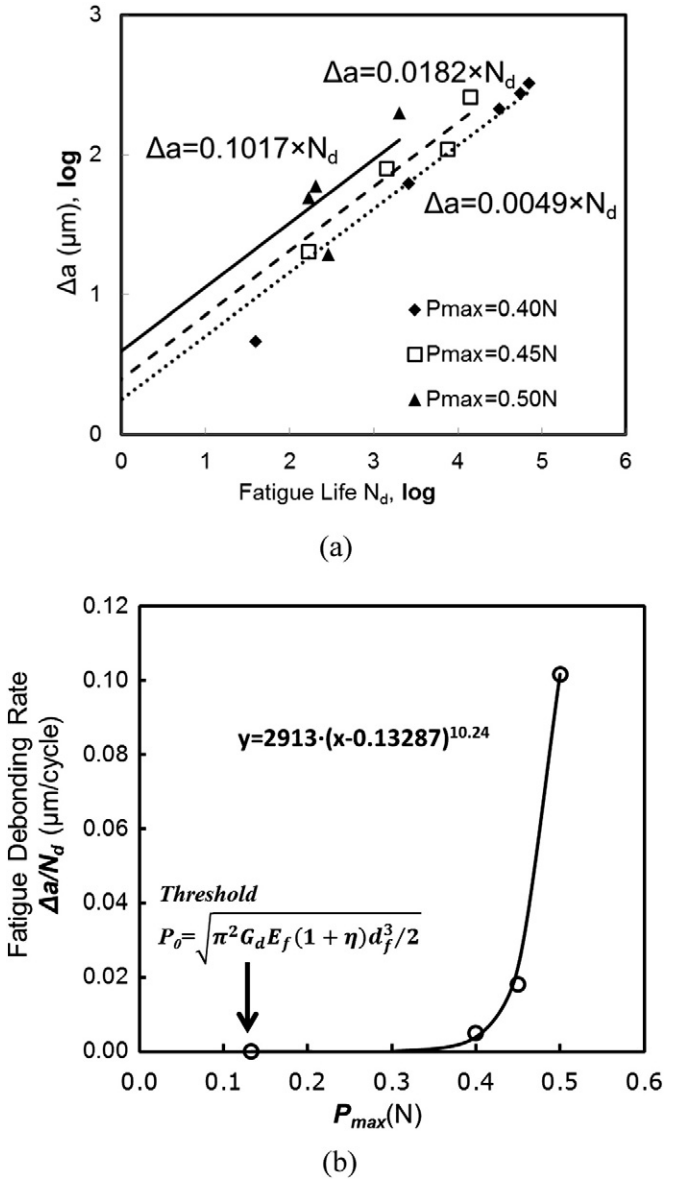

Fig. 3. (a) Fatigue-induced fiber debonding, i.e. tunnel crack propagation Δa, as a function of fatigue cycle (N_d) and fatigue loading level (P_{max}); and (b) fatigue-induced fiber debonding rate ($\Delta a/N_d$) as a function of P_{max} [20].

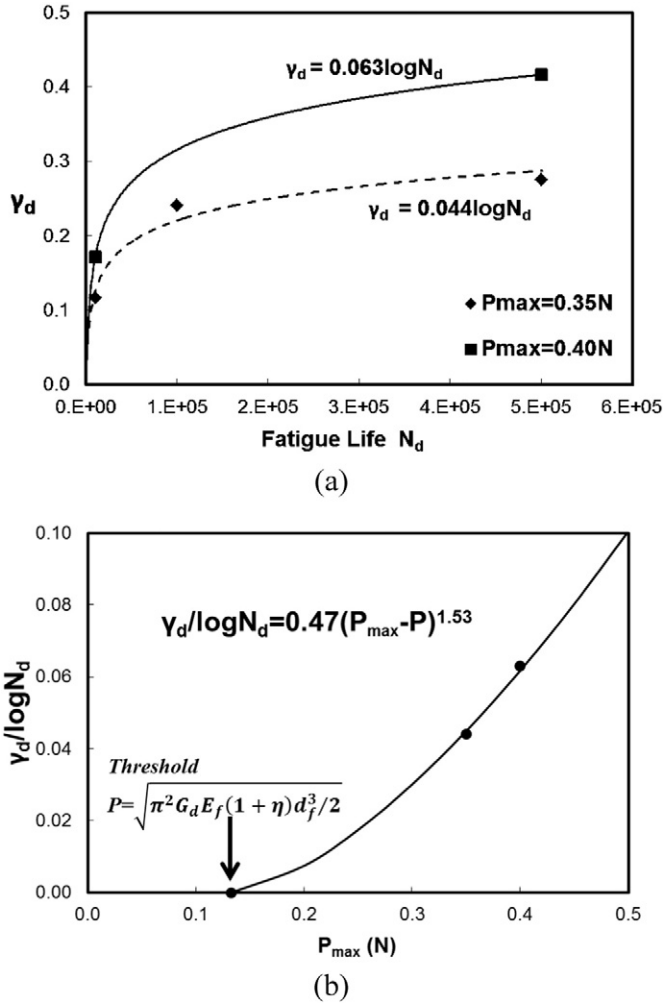

Fig. 4. *Fatigue debonding hardening* coefficient γ_d as a function of fatigue cycle N_d and fatigue load level P_{max} [20].

or interface debris accumulation along the tunnel crack between the fiber-matrix interface. This leads to an increasing load resisting fiber pullout.

In current model, the increase of frictional bond in the debonding stage is captured by introducing the *fatigue debonding hardening* coefficient γ_d which is a function of fatigue loading level P_{max} and fatigue cycle N_d as shown in Eq. 12.

$$\tau = \tau_0[1 + \gamma_d(N_d, P_{max})] \tag{12}$$

where τ_0 is the frictional bond and τ is the fatigue-enhanced frictional bond due to debonding hardening. τ_0 and τ can be measured experimentally as illustrated in [20] where a micro-PVA fiber was pulled out from a mortar matrix and γ_d (N_d, P_{max}) can be derived accordingly. Fig. 4 shows that γ_d increases with the fatigue load cycle N_d in a logarithmic manner, and the increasing rate γ_d / $logN_d$ is correlated with P_{max}. It should be noted that in Fig. 4b, there also exists a threshold P to initiate fatigue debonding, only after which the *fatigue debonding hardening* effect can occur. As a result, γ_d (N_d, P_{max}) is given in the form of Eq. 13

$$\gamma_d = \begin{cases} C_d \cdot \left(P_{max} - \sqrt{\pi^2 G_d E_f (1+\eta) d_f^3/2}\right)^{M_d} \cdot logN_d, & N_d \geq 1 \\ 0, & N_d = 0 \end{cases} \tag{13}$$

The details of the experimental program and discussions on the *fatigue debonding hardening* in PVA fiber-reinforced cement system can be found in [20].

3.1.3. Fatigue dependent single fiber pullout behavior during the debonding stage

The analytical solution of fatigue dependent single fiber pullout behavior during the debonding stage, i.e. $P(u, N_d, P_{max})$, is given in Eq. 14.

$$P = \begin{cases} \pi E_f d_f^2 u/4a + \pi\tau a d_f(1+\eta)/2, & u<u' \\ \pi(\tau-\tau_0)a d_f(1+\eta) + \pi d_f\sqrt{\dfrac{E_f d_f(G_d + u\tau_0)(1+\eta)}{2} - a^2\tau_0(\tau-\tau_0)(1+\eta)^2}, & u'<u<u'_0 \end{cases} \tag{14}$$

where a is the fatigue-induced fatigue debonding length which can be determined from Eq. 10; τ is the frictional bond in the fatigue debonded interface considering fatigue debonding hardening which can be determine from Eq.; u' is the corresponding fiber pullout displacement when P reaches the critical value initiating further interface debonding; and u_0' is the corresponding fiber pullout displacement when fiber is fully

debonded. The value of u' and u_0' are given in Eqs. 15 and 16, respectively. The derivation of Eqs. 14–16 can be found in Appendix A.

$$u' = \frac{2\tau a^2(1+\eta)}{E_f d_f} + a\sqrt{\frac{8G_d(1+\eta)}{E_f d_f}} \tag{15}$$

$$u_0' = \frac{2\left(\tau_0 L_e^2 + \tau a^2 - \tau_0 a^2\right)(1+\eta)}{E_f d_f} + L_e\sqrt{\frac{8G_d(1+\eta)}{E_f d_f}} \tag{16}$$

3.2. Fatigue dependent fiber slippage process

In the fatigue single fiber pullout experiment of [20] where a micro-PVA fiber was pulled out from a mortar matrix, it has been shown that when the fatigue loading level P_{max} was higher than the P_a, the full-debonding of fiber was completed even before the first cycle of fatigue loading. The fatigue deterioration in the slippage stages can be characterized with such cases. Specifically, the *fatigue slippage hardening* must be added into the new model.

3.2.1. Fatigue slippage hardening

At high-level fatigue ($P_{max} > P_a$), it was found that the chemical bond G_d between fiber and matrix diminished, and the frictional bond τ_0 was enhanced with fatigue cycle applied during slippage stage N_s and fatigue loading level P_{max} [20]. Such enhancement was referred as *fatigue slippage hardening*. Similar to *fatigue debonding hardening*, this phenomenon can also be attributed to the jamming effect between the fiber and matrix, which results from the fiber damage accumulated during the reciprocated movement.

In current model, the fatigue dependent frictional bond in the slippage stage is given as shown in Eq. 17.

$$\tau = \tau_0\left[1 + \beta(u-u_0)/d_f\right]\left[1 + \gamma_d(N_d, P_{max})\right]\left[1 + \gamma_s(N_s, P_{max})\right] \tag{17}$$

where τ_0 is the frictional bond, γ_s is the *fatigue slippage hardening* coefficient which is a function of fatigue loading level P_{max} as well fatigue cycle N_s, and τ is the fatigue-enhanced frictional bond due to the debonding and slippage hardening. τ_0, τ, and β can be measured experimentally as illustrated in [20] where a micro-PVA fiber was pulled out from a mortar matrix and γ_s (N_s, P_{max}) can be derived accordingly. Fig. 5 shows that γ_s increases with the fatigue load cycles N_s in a logarithmic manner, and the increasing rate $\gamma_s/logN_s$ is correlated with the power of P_{max}. As a result, γ_s is given in the form of Eq. 18.

$$\gamma_s = \begin{cases} C_s \cdot {P_{max}}^{M_s} \cdot logN_s, & N_s \geq 1 \\ 0, & N_s = 0 \end{cases} \tag{18}$$

where C_s and M_s are material related constants. The details of the experimental program and discussions on the *fatigue slippage hardening* in PVA fiber-reinforced cement system can be found in [20].

3.2.2. Fatigue dependent single fiber pullout behavior during the slippage stage

The analytical solution of fatigue dependent single fiber pullout behavior during the slippage stage, i.e. $P(u, N_s, P_{max})$ where $u > u_o$, considering *fatigue slippage hardening* can therefore be determined as Eq. 19.

$$P = \pi d_f \tau (L_e + u_0 - u)\left[1 + \frac{\beta(u-u_0)}{d_f}\right], \quad u \geq u_0 \tag{19}$$

where τ can be determined from Eq. 16 where both the fatigue debonding hardening and fatigue slippage hardening are considered by introducing γ_d and γ_s, respectively. The fiber full-debonding could occur during the fatigue loading, which divides the total number of load cycles N into N_d and N_s, in such situation the effect of *fatigue debonding hardening* and *fatigue slippage hardening* must be considered separately. If the fatigue loading level P_{max} is large enough to fully debond the fiber during the first cycle, γ_d will be zero. N_d and N_s can be determined by Eqs. 20 and 21 respectively.

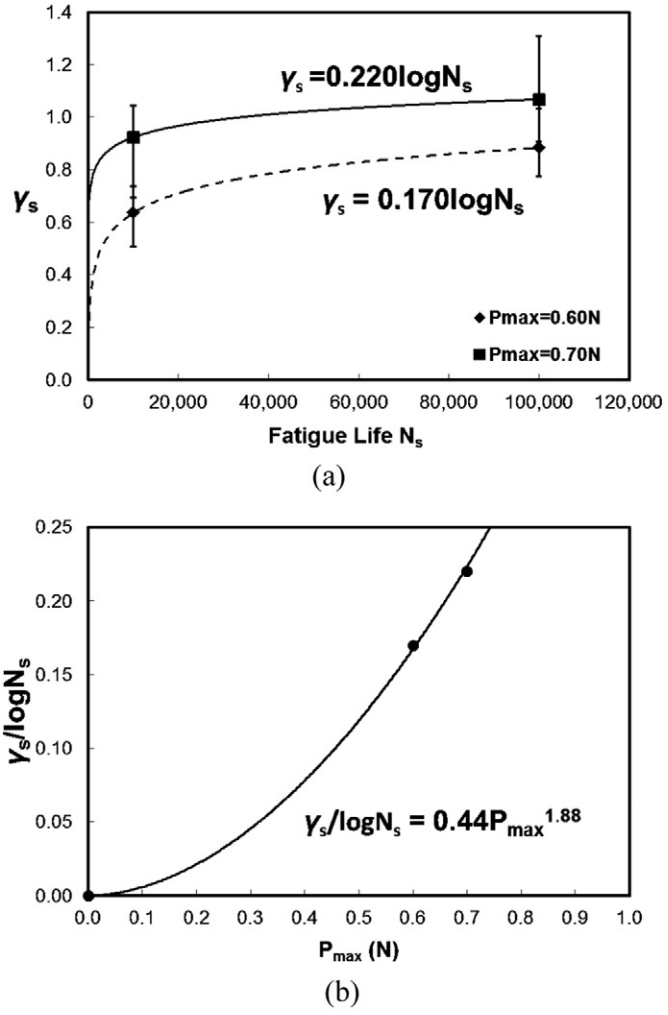

Fig. 5. *Fatigue slippage hardening* coefficient γ_s as a function of fatigue cycle N_s and fatigue load level P_{max} [20].

$$N_d = \begin{cases} N, & N < N_{d0} \\ N_{d0}, & N > N_{d0} \end{cases} \tag{20}$$

$$N_s = N - N_d \tag{21}$$

where N_{d0} is the number of cycle needed to fully debond the fiber from matrix and calculated as Eq. 22.

$$N_{d0} = \begin{cases} 1, & a_0(P_{max}) > L_e \\ (L_e - a_0)/\left(C \cdot {P_{max}}^{M}\right), & a_0(P_{max}) < L_e \end{cases} \tag{22}$$

4. Macro-scale modeling: Fatigue dependent fiber-bridging constitutive law

The fatigue dependent single fiber load-displacement (P-u) relation has been characterized and modelled in the previous section. On the macro-scale, once the crack occurs, the total stress is sustained by all fibers bridged across the crack. As a result, the fatigue dependent fiber-bridging σ-δ relation can be obtained by summing the load carried by the individual fibers under given crack opening.

4.1.1. Snubbing effect

In single fiber pullout model, the fiber embedment length L_e is predetermined and the fiber orientation φ (the angle between fiber alignment and tensile loading) is 0°. In the fiber-bridging model, however, the randomness of fiber distribution must be considered by varying L_e and φ. It has been reported that misaligned fiber ($\varphi \neq 0$) is subjected to additional load due to the Euler friction pulley effect at the fiber exit point, and new $P(\varphi)$ can be calculated as suggested by [25].

$$P(\varphi) = P(\varphi = 0) \cdot e^{f\varphi} \tag{23}$$

where $f > 0$ is referred as snubbing coefficient. The effects of fatigue loading on the snubbing coefficient remained unknown. For simplicity, snubbing coefficient was assumed to be independent to the fatigue loading in the current model. Similar assumption was also adopted in Li and Matsumoto's model [17,18].

4.1.2. Fatigue-induced deterioration of in-situ fiber strength

When accounting the force resistance by individual fibers, fiber rupture must be considered by introducing the in-situ fiber strength, σ_{fu}. It has been reported that the in-situ fiber strength is a function of fiber orientation [26,27]. The in-situ fiber strength is also affected by the fatigue load cycles as reported previously by the authors [19]. Fig. 6 shows that in-situ σ_{fu} of a micro-PVA fiber decreasing linearly with fatigue load cycles, for both 0°- and 30°-oriented embedded fiber. As a result, σ_{fu} can be expressed as a function of orientation and fatigue cycle.

$$\sigma_{fu}(\varphi, N) = \sigma_{fu}(\varphi = 0, N = 1) \cdot e^{-f'\varphi} \cdot \left[1 - f'' \cdot \log(N)\right] \tag{24}$$

where $f' > 0$ and $f'' > 0$ are referred as fiber strength reduction coefficients due to fiber orientation and fatigue cycle, respectively.

4.1.3. Randomness of fiber distribution

The randomness of L_e and φ can be accounted by adopting probability density functions $p(z)$ and $p(\varphi)$, where z is the distance from fiber geometrical center to the crack surface, and $L_e = L_f/2\text{-}z$. [22,26] suggested that $p(z)$ and $p(\varphi)$ can be calculated as Eqs. 25 and 26 respectively:

$$p(z) = 2/L_f, \quad 0<z<L_f/2 \tag{25}$$

$$p(\varphi) = \begin{cases} 2/\pi, & 0<\varphi<2/\pi, \quad 2D\ fiber\ distribution \\ \sin(\varphi), & 0<\varphi<2/\pi, \quad 3D\ fiber\ distribution \end{cases} \tag{26}$$

where the 2D fiber distribution is applied to the FRCC specimen whose smallest dimension is comparable to the fiber length; and the 3D fiber distribution is applied to the FRCC specimen whose smallest dimension is much larger than the fiber length.

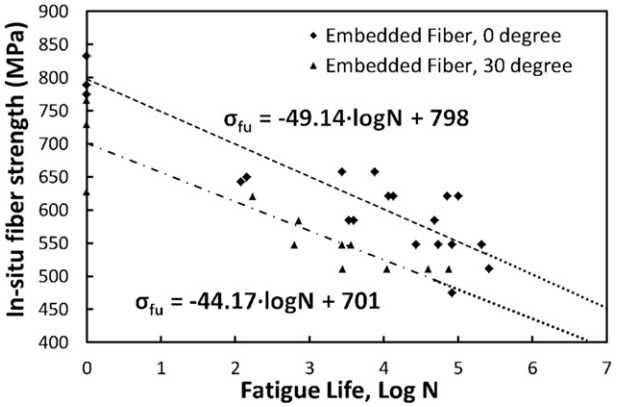

Fig. 6. Fatigue-induced deterioration of in-situ fiber strength [19].

4.1.4. Averaging

For a given cross section area of specimen A, the number of fibers N_f for within a specific range of L_e (z_1 to z_2) and φ (φ_1 to φ_2) can be calculated as Eq. 27.

$$N_f = \frac{A}{A_f} \cdot V_f \cdot \int_{\varphi_1}^{\varphi_2} \int_{z_1 \cos\varphi}^{z_2 \cos\varphi} p(\varphi) p(z) dz d\varphi \tag{27}$$

where A_f is the cross section area of an individual fiber and V_f is the fiber content fraction by volume. The total number of fibers crossing the crack can be calculated when adopting $z_1 = 0, z_2 = L_f/2, \varphi_1 = 0$, and $\varphi_2 = \pi/2$.

With the aforementioned formula for the fatigue dependent single fiber pullout behavior (Eqs. 8–21), the fatigue dependent fiber-bridging constitutive model, i.e. $\sigma(\delta, N, \sigma_{max})$ where N is the number of load cycles, σ_{max} is the ambient fatigue tensile stress, can be computed with a numerical procedure illustrated in Fig. 7.

5. Results and discussion

The modeling results of fatigue dependent single-fiber pullout behavior are compared against the experimental measurements to verify the validity of the new model. The micromechanical parameters as the input of the model are given in Table 1. Single-fiber pullout curves after two different fatigue loading schemes are included in Fig. 8. In the experimental study, when the fatigue loading level was relatively low ($P_{max} < 0.4$ N), the full-debonding was never reached during the fatigue preloading and the load drop from P_a to P_b at $u = u_0$ during monotonic reloading still existed. When the fatigue loading level was relatively high ($P_{max} > 0.5$ N), the full-debonding had been reached during the fatigue preloading and the load drop during monotonic reloading was not observed. In can be seen in Fig. 8a and b, both effects can be well captured by the current model. In the first stage of Eq. 14, it is noticed that the tensile force P must reach a certain level to overcome the frictional bond, which is quantified by the second term in Eq. 9. The fiber displacement u can be activated after only the frictional bond is overcome, which is reflected in the modeling curve Fig. 8. However, the experimental P-u curve initiates from (0,0) as the stretch of the free fiber was inevitable in the actual testing [20]. Table 2 compares the P_a and P_b measured in the experimental study and those predicted by the current model at different fatigue loading levels and fatigue cycles. It can be seen that the value of P_a and P_b can be well predicted after various fatigue preloading schemes.

The fiber-bridging σ-δ curves in typical PVA fiber-reinforced cementitious composites, after fatigue deterioration of different fatigue cycle (N) at different loading level (σ_{max}), were predicted with the current model. The input parameters were given in Table 1. Two types of PVA fibers, with and without surface oil-treatment, were considered. Previous studies [19,20] have shown that oil-treatment can effectively mitigate the fatigue deterioration of the fiber and fiber-matrix interface.

Figs. 9 and 10 show the post-fatigue fiber-bridging curves of non-oil-coated and oil-coated PVA fiber systems. It can be seen that for both systems, the fiber bridging gradually deteriorates with increasing number of fatigue cycles (Figs. 9a and 10a). Specifically, the ascending part of the curve is gradually enhanced with fatigue loading because of the *fatigue debonding hardening* and *fatigue slippage hardening* effects on the micro-scale. On the other hand, the peak of the curve, i.e. σ_0, gradually decreases with fatigue, which is attributed to the premature fiber rupture due to the interface hardening as well as the fatigue deterioration of the in-situ strength of fiber. As a result of the fiber-bridging deterioration, the energy dissipation, which is reflected by the area under the σ-δ curve, is also decreased. It is also notice that the degree of fiber-bridging deterioration depends on the fatigue loading level σ_{max} (Figs. 9b and 10b), which reflects the micro-scale observation that the fatigue-dependency of fiber strength and fiber-matrix interface hardening is related to the fatigue loading level P_{max}.

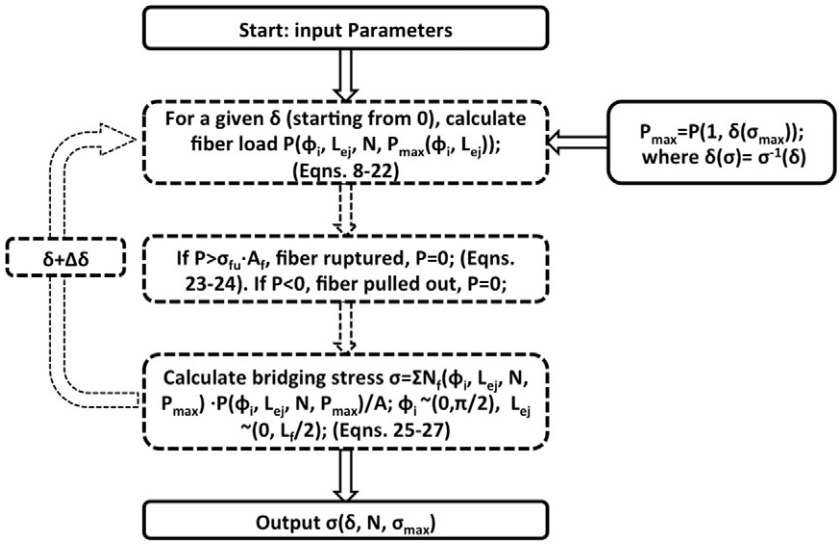

Fig. 7. Flow chart of the numerical procedure for computing FRCC fiber-bridging constitutive law $\sigma(\delta, N, \sigma_{max})$.

Fig. 11 compares the post-fatigue fiber bridging with non-oil-coated and oil-coated PVA fibers. It can be seen that despite the slightly lower σ_0, the fiber surface oil-treatment can greatly delay the failure of the fiber bridging and enhance the load capacity of the descending part of the curve. Therefore, the oil-treatment enlarges the energy dissipation capacity of the fiber-bridging. Such changes on the macro-scale can be attributed to that on the micro-scale oil-coating reduces the fatigue-induced fiber-matrix interface hardening [20] as well as the fiber strength reduction [19], as a result more fibers sustain instead of rupture during the widening of δ.

While the current model is verified with the experimental results of PVA fiber-reinforced cementitious composites, where the fiber-matrix interface undergoes hardening under fatigue loading, it may also be applied to other fiber-reinforced cementitious composites, where the

Table 1
Micromechanical parameters for the calculation of fatigue dependent single-fiber pullout curve and fatigue dependent fiber-bridging constitutive law.

Input parameters		Notation	Non-oil-coated PVA fiber	Oil-coated PVA fiber
Monotonic micro-scale parameters	Fiber Young's modulus	E_f (GPa)	22*	22
	Fiber diameter	d_f (mm)	39*	39
	Fiber fraction	V_f (%)	2	2
	Matrix Young's modulus	E_m (GPa)	20*	20
	Chemical bond	G_d (J/m^2)	2.68*	1.77
	Frictional bond	τ_0 (MPa)	1.89*	1.37
	Slip-hardening coefficient	β	0.19*	0.21
	Snubbing coefficient	f	0.2	0.2
	Fiber strength reduction coefficient (orientation)	f'	0.33	0.33
Fatigue dependent micro-scale parameters	Fatigue-debonding coefficients	C	0.002913*	0.002659
		M	10.24*	10.88
	Interfacial hardening coefficients	C_d	0.47*	0.46
		M_d	1.53*	1.93
		C_s	0.44*	0.39
		M_s	1.88*	1.87
	Fiber strength reduction coefficient (fatigue)	f'	0.0649	0.0536

* used as input parameters for calculating the post-fatigue single-fiber pull out curve in Fig. 8.

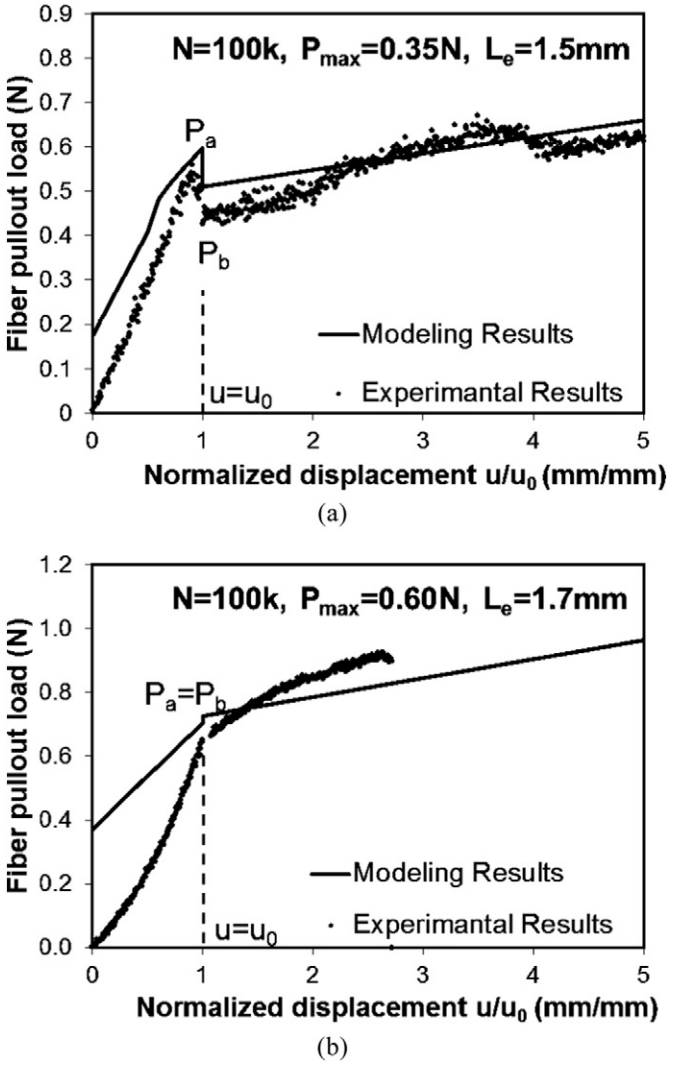

Fig. 8. Measured and modelled post-fatigue single-fiber pullout behavior (P-u curve): (a) low level fatigue where full-debonding has not completed during fatigue ($P_{max} = 0.35$ N); and (b) high level fatigue where full-debonding has occurred during the loading ramping stage before 1st fatigue cycle ($P_{max} = 0.60$ N).

Table 2
P_a and P_b after fatigue preloading: the modeling results vs. the experimental results.

	P_{max} (N)	Load cycles N	P_a (N)		P_b (N)	
			Experimental	Modeling	Experimental	Modeling
No fully-debonded	0.35	10,000	0.513 ± 0.051	0.546	0.388 ± 0.043	0.445
	0.35	100,000	0.565 ± 0.031	0.571	0.431 ± 0.035	0.476
	0.35	500,000	0.592 ± 0.039	0.610	0.443 ± 0.043	0.497
	0.40	10,000	0.521 ± 0.050	0.591	0.407 ± 0.062	0.473
Fully-debonded	0.50	10,000	0.537 ± 0.021	0.544	$=P_a$	
	0.60	10,000	0.640 ± 0.020	0.576		
	0.60	100,000	0.655 ± 0.021	0.604		
	0.70	10,000	0.740 ± 0.034	0.616		
	0.70	100,000	0.794 ± 0.008	0.689		

fiber-matrix interface undergoes softening under fatigue loading such as steel fiber [28]. In the current model, the interfacial hardening behavior is captured by the two hardening coefficients γd and γs, a fiber-matrix interface with softening behavior can also be described by using these two coefficients with negative values. Further verification with experimental results is preferred before the current model being used in different fiber-matrix systems.

6. Conclusions

This paper proposes a novel multi-scale analytical model to predict the fatigue deterioration of the fiber bridging (σ-δ curve) in fiber-reinforced cementitious composites (FRCC). On the micro-scale, a new analytical model to predict the post-fatigue single-fiber pullout behavior (P-u curve) is established based on the understanding of the fatigue

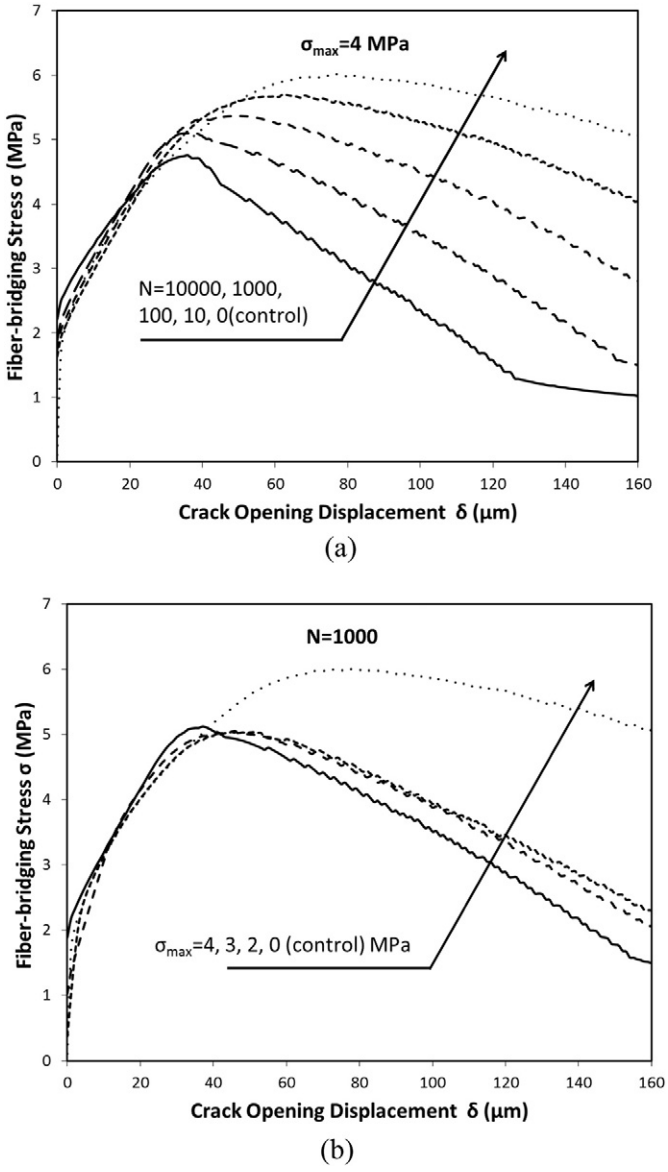

Fig. 9. (a) Effects of fatigue cycle N; and (b) effects of fatigue load level σ_{max} on modelled $\sigma(\delta)$ of non-oil-coated PVA fiber FRCC.

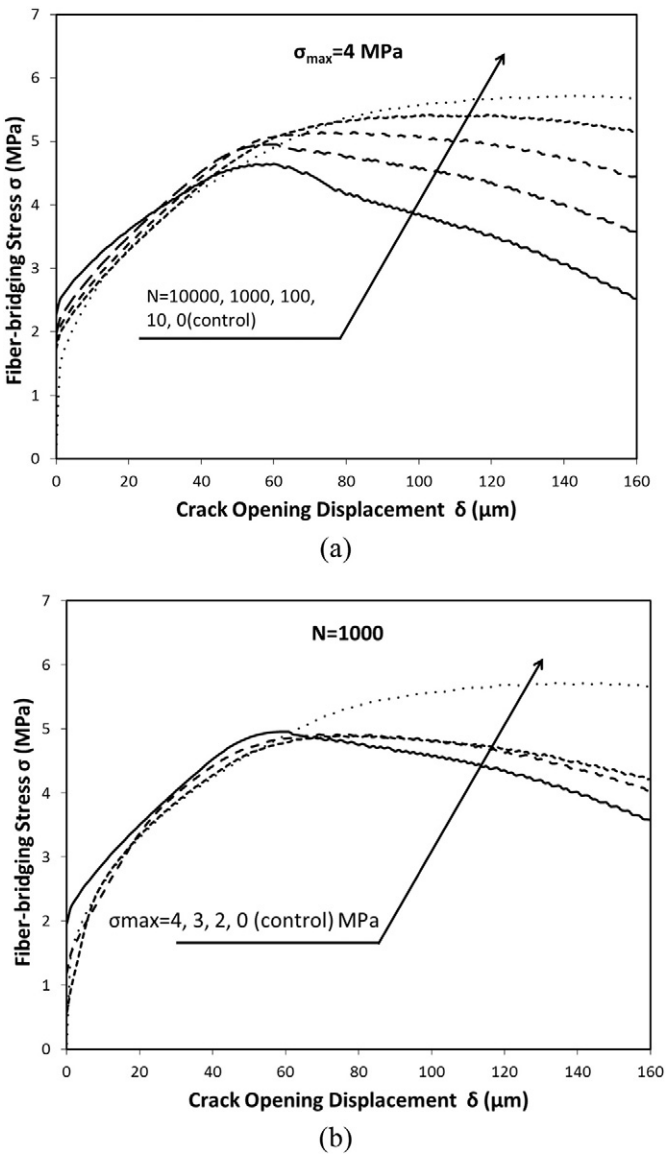

Fig. 10. (a) Effects of fatigue cycle N; and (b) effects of fatigue load level σ_{max} on modelled $\sigma(\delta)$ of oil-coated PVA fiber FRCC.

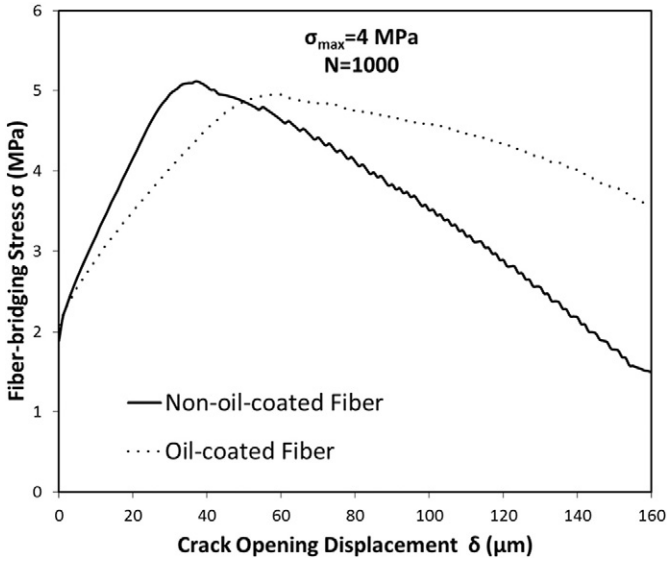

Fig. 11. Comparison of the fiber bridging constitutive laws with oil-coated and non-oil-coated PVA fibers after fatigue deterioration ($N = 1000$ cycles and $\sigma_{max} = 4$ MPa).

dependency of fiber and fiber-matrix interface. On the macro-scale, the fatigue-induced fiber strength reduction was considered and probabilistics is introduced to describe the randomness of fiber location and orientation with respect to crack plane. The random orientation of fiber also necessitates the accounting of the mechanics of interaction between an inclined fiber and the matrix crack so that the fatigue dependent fiber-bridging constitutive law can be predicted. The model proposed in this paper is the first analytical model that is able to capture the effects of fatigue cycle (N) as well as the fatigue loading level (σ_{max}) on deterioration of fiber bridging in FRCC.

Acknowledgement

This work was supported by the SinBerBEST [NRFCRP8-2011-03] program and National Research Foundation of Singapore [COE_SUG/RSS_19MAR10_1/23].

Appendix A. Derivation of *P-u* relation ($u < u < u_0'$) after fatigue-induced debonding and fatigue debonding hardening

Fig. A1Illustration of a fiber being pulled out from matrix after fatigue loading.

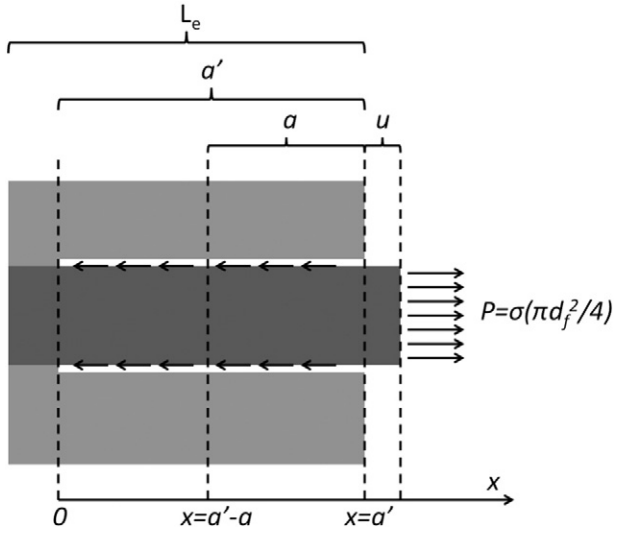

Fig. A1 illustrates the process of single fiber being pulled out by monotonic loading after it was pre-debonded by fatigue loading. In Fig. A1, the new fiber debonding has been triggered, or in other words, the current debonding crack length a' is larger than a, the crack length immediately after fatigue loading. At the debonded interface, the frictional bond is τ_0 if $0 < x \le a' - a$ and τ if $a' - a < x \le a'$.

Taking the free-body diagram of the debonded fiber ($0 < x \le a' - a$), it is not hard to get Eqs. A1 and A2 based on force equilibrium.

$$\frac{d\sigma_{f1}(x)}{dx} = \frac{4\tau_0}{d_f} \tag{A1}$$

$$\frac{d\sigma_{f2}(x)}{dx} = \frac{4\tau}{d_f} \tag{A2}$$

where $\sigma_{f1}(x)$ and $\sigma_{f2}(x)$ represent the cross-sectional tensile stress in the fiber, and the subscript "1" and "2" indicates the new generated debonding length ($0 < x \le a' - a$) and the debonding length by fatigue ($a' - a < x \le a'$). Then integrate both equations and take the boundary conditions in Eqs. A3 and A4.

$$\sigma_{f1}(a'-a) = \sigma_{f2}(a'-a) \tag{A3}$$

$$\sigma_{f2}(a') = \sigma \tag{A4}$$

where σ is the cross-sectional tensile stress at the fiber free end. The expressions of $\sigma_{f1}(x)$ and $\sigma_{f2}(x)$ can be solved and given in Eqs. A5 and A6.

$$\sigma_{f1}(x) = \frac{4\tau_0 x}{d_f} + \sigma + \frac{4(\tau-\tau_0)(a'-a)-4\tau a'}{d_f}, \quad 0<x<a'-a \tag{A5}$$

$$\sigma_{f2}(x) = \frac{4\tau x}{d_f} + \sigma - \frac{4\tau a'}{d_f}, \qquad a'-a<x<a' \tag{A6}$$

Taking the free-body length of the composites, i.e. fiber and matrix together and consider the force equilibrium (Eq. A7), the cross-sectional tensile stress in the matrix $\sigma_m(x)$ can be calculated as Eqs. A8 and A9.

$$V_f\sigma_f(x) + (1-V_f)\sigma_m(x) = V_f\sigma \tag{A7}$$

$$\sigma_{m1}(x) = \left(\frac{V_f}{1-V_f}\right)\left[-\frac{4\tau_0 x}{d_f} - \frac{4(\tau-\tau_0)(a'-a)-4\tau a'}{d_f}\right], \quad 0<x<a'-a \tag{A8}$$

$$\sigma_{m2}(x) = \left(\frac{V_f}{1-V_f}\right)\left[-\frac{4\tau x}{d_f} + \frac{4\tau a'}{d_f}\right], \qquad a'-a<x<a' \tag{A9}$$

The relative displacement between the fiber and the matrix can be calculated as Eqs. A10 and A11.

$$\Delta_1(x) = \int_0^x \left[\frac{\sigma_{f1}(x)}{E_f} - \frac{\sigma_{m1}(x)}{E_m}\right]dx, \quad 0<x<a'-a \tag{A10}$$

$$\Delta_2(x) = \int_0^{a'-a}\left[\frac{\sigma_{f1}(x)}{E_f} - \frac{\sigma_{m1}(x)}{E_m}\right]dx + \int_{a'-a}^{x}\left[\frac{\sigma_{f2}(x)}{E_f} - \frac{\sigma_{m2}(x)}{E_m}\right]dx, \quad 0<x<a'-a \tag{A11}$$

The relative displacement of the fiber free end to matrix u can be calculated as Eq. A12 by taking x as a'.

$$u = \int_0^{a'-a}\left[\frac{\sigma_{f1}(x)}{E_f} - \frac{\sigma_{m1}(x)}{E_m}\right]dx + \int_{a'-a}^{a'}\left[\frac{\sigma_{f2}(x)}{E_f} - \frac{\sigma_{m2}(x)}{E_m}\right]dx \tag{A12}$$

or

$$u = \frac{\sigma a'}{E_f} + \frac{2(1+\eta)\left[(\tau-\tau_0)(a'-a)^2 - \tau a'^2\right]}{E_f d_f} \tag{A13}$$

where $\eta = E_f V_f / E_m(1 - V_f)$.

Based on the fracture mechanics concept, the energy criterion for debonding crack advancing is given in Eq. A14.

$$G_d \pi d_f da' = dW - dW_\varepsilon - dW_f \tag{A14}$$

where dW, dW_ε, and dW_f are the external work, strain energy, and friction-induced energy dissipation while the crack advancing by da. The calculation of dW and dW_ε, can be rewritten as Eqs. A15 and A16 respectively.

$$dW = P du_f \tag{A15}$$

$$dW_\varepsilon = \frac{P du_f - dW_f}{2} \tag{A16}$$

where u_f is the displacement of the fiber free end. As a result, the energy balance can be rewritten as Eq. A17.

$$G_d \pi d_f da' = \frac{P du_f - dW_f}{2} \tag{A17}$$

Now it is to quantify u_f as well as W_f. u_f is a combination of the elongation of the debonded part of fiber and the elongation of the undebonded composite, which includes fiber and matrix. As a result, u_f is calculated as Eq. A18.

$$u_f = \int_0^{a'-a}\left[\frac{\sigma_{f1}(x)}{E_f}\right]dx + \int_{a'-a}^{a'}\left[\frac{\sigma_{f2}(x)}{E_f}\right]dx + \frac{V_f\sigma(L_e - a')}{E_d} \tag{A18}$$

where $\sigma_{f1}(x)$ and $\sigma_{f2}(x)$ are calculated with Eqs. A5 and A6. W_f, on the other hand, is calculated in Eq. A19.

$$W_f = \int_0^{a'-a}\left[\pi d_f \tau_0 \Delta_1(x)\right]dx + \int_{a'-a}^{a'}\left[\pi d_f \tau \Delta_2(x)\right]dx \tag{A19}$$

where $\Delta_1(x)$ and $\Delta_2(x)$ are calculated with Eqs. A10 and A11. Combining Eqs. A17–19, the relation between σ and a' can be obtained as Eq. A20.

$$\sigma^2 - \frac{8(1+\eta)[\tau_0 a' + (\tau-\tau_0)a]}{d_f}\sigma + \frac{16(1+\eta)^2[(\tau-\tau_0)(a'-a) - \tau a']^2}{d_f^2} - \frac{8(1+\eta)G_d E_f}{d_f} = 0 \tag{A20}$$

By solving this equation, $\sigma(a')$ is calculated as Eq. A21.

$$\sigma(a') = \frac{4(1+\eta)\tau_0 a' + 4(1+\eta)(\tau-\tau_0)a + \sqrt{8(1+\eta)G_d E_f d_f}}{d_f} \tag{A21}$$

Eqs. A13 and A21 are two critical relation that summarize the relation between σ, u, and a. They are derived based on force equilibrium and energy criterion respectively. By taking Eq. A21 into Eq. A13, $u(a')$ is obtained as Eq. A22.

$$u(a') = \frac{2(1+\eta)\left[(\tau-\tau_0)a^2 + \tau_0 a'^2\right] + a'\sqrt{8(1+\eta)G_d E_f d_f}}{E_f d_f} \tag{A22}$$

When $a' = a$ and $a' = L_e$, Eqs. 15 and 16 are obtained. By combining Eqs. A21 and A22 and taking account of $P = \sigma(\pi d_f^2)/4$, the second mathematical expression of Eq. 14 can be obtained.

References

[1] T.F. Fwa, The Handbook of Highway Engineering, CRC Press, 2005.
[2] K. Okada, H. Okamura, K. Sonoda, Fatigue failure mechanism of reinforced concrete bridge deck slabs, Transp. Res. Rec. 664 (1978) 136–144.
[3] W. Ferdous, A. Manalo, Failures of mainline railway sleepers and suggested remedies–review of current practice, Eng. Fail. Anal. 44 (2014) 17–35.
[4] R. Harte, G.P. Van Zijl, Structural stability of concrete wind turbines and solar chimney towers exposed to dynamic wind action, J. Wind Eng. Ind. Aerodyn. 95 (2007) 1079–1096.
[5] M. Lee, B. Barr, An overview of the fatigue behaviour of plain and fibre reinforced concrete, Cem. Concr. Compos. 26 (2004) 299–305.
[6] C.D. Johnston, R.W. Zemp, Flexural fatigue performance of steel fiber reinforced concrete—influence of fiber content, aspect ratio, and type, ACI Mater. J. 88 (1991) 374–383.
[7] S. Singh, S. Kaushik, Flexural fatigue analysis of steel fiber-reinforced concrete, ACI Mater. J. 98 (2001) 306–312.
[8] Y. Mohammadi, S. Kaushik, Flexural fatigue-life distributions of plain and fibrous concrete at various stress levels, J. Mater. Civ. Eng. 17 (2005) 650–658.
[9] K. Tawfiq, J. Amaghani, R. Ruiz, Fatigue cracking of polypropylene fiber reinforced concrete, ACI Mater. J. 96 (1999) 226–233.
[10] J. Jang, H. Kim, T. Kim, B. Min, H. Lee, Improved flexural fatigue resistance of PVA fiber-reinforced concrete subjected to freezing and thawing cycles, Constr. Build. Mater. 59 (2014) 129–135.
[11] H. Li, M.-H. Zhang, J.-P. Ou, Flexural fatigue performance of concrete containing nano-particles for pavement, Int. J. Fatigue 29 (2007) 1292–1301.
[12] Y. Lv, H.-M. Cheng, Z.-G. Ma, Fatigue performances of glass fiber reinforced concrete in flexure, Procedia Engineering 31 (2012) 550–556.
[13] Z. Deng, The fracture and fatigue performance in flexure of carbon fiber reinforced concrete, Cem. Concr. Compos. 27 (2005) 131–140.
[14] A. Naaman, H. Hammoud, Fatigue characteristics of high performance fiber-reinforced concrete, Cem. Concr. Compos. 20 (1998) 353–363.
[15] J. Zhang, H. Stang, V.C. Li, Experimental study on crack bridging in FRC under uniaxial fatigue tension, J. Mater. Civ. Eng. 12 (2000) 66–73.
[16] J. Zhang, H. Stang, V.C. Li, Fatigue life prediction of fiber reinforced concrete under flexural load, Int. J. Fatigue 21 (1999) 1033–1049.
[17] V.C. Li, T. Matsumoto, Fatigue crack growth analysis of fiber reinforced concrete with effect of interfacial bond degradation, Cem. Concr. Compos. 20 (1998) 339–351.
[18] T. Matsumoto, V.C. Li, Fatigue life analysis of fiber reinforced concrete with a fracture mechanics based model, Cem. Concr. Compos. 21 (1999) 249–261.
[19] J. Qiu, E.-H. Yang, Study on fatigue failure of polymeric fiber-reinforced strain-hardening cementitious composites, in: E. Schlangen (Ed.), 3rd International RELIM Conference on Strain Hardening Cementitious Composites, Dordrecht, Netherlands Nov, 2014, pp. 3–5.
[20] J. Qiu, E.-H. Yang, Micromechanics-based study on fatigue failure of engineered cementitious composites, in: H.W. Reinhardt (Ed.), 7th RILEM Workshop on High Performance Fiber Reinforced Cement Composites, Stuttgart, Germany Jun, 2015, pp. 1–3.
[21] C. Redon, V.C. Li, C. Wu, H. Hoshiro, T. Saito, A. Ogawa, Measuring and modifying interface properties of PVA fibers in ECC matrix, J. Mater. Civ. Eng. 13 (2001) 399–406.
[22] Z. Lin, T. Kanda, V.C. Li, On interface property characterization and performance of fiber reinforced cementitious composites, Concr. Sci. Eng. 1 (1999) 173–184.
[23] Z. Lin, V.C. Li, Crack bridging in fiber reinforced cementitious composites with slip-hardening interfaces, Journal of the Mechanics and Physics of Solids 45 (1997) 763–787.
[24] L. Pook, N. Frost, A fatigue crack growth theory, Int. J. Fract. 9 (1973) 53–61.
[25] J. Morton, G. Groves, The effect of metal wires on the fracture of a brittle-matrix composite, J. Mater. Sci. 11 (1976) 617–622.
[26] E.-H. Yang, S. Wang, Y. Yang, V.C. Li, Fiber-bridging constitutive law of engineered cementitious composites, J. Adv. Concr. Technol. 6 (2008) 181–193.
[27] T. Kanda, V.C. Li, Interface property and apparent strength of high-strength hydrophilic fiber in cement matrix, J. Mater. Civ. Eng. 10 (1998) 5–13.
[28] J. Zhang, H. Stang, V.C. Li, Crack bridging model for fiber reinforced concrete under fatigue tension, Int. J. Fatigue 23 (2001) 655–670.